Weight of an Hourglass – Theory and Experiment in Quantitative Comparison

Achim Sack and Thorsten Pöschel
Institute for Multiscale Simulation, Universität Erlangen-Nürnberg, Nägelsbachstraße 49b, 91052 Erlangen, Germany
(Dated: March 3, 2016)

A flowing hourglass changes its weight in the course of time because of the accelerated motion of its center of mass. While this insight is not new, it is frequently said that the effect is tiny and hardly measurable. Here we present a simple experiment which allows to monitor the weight as a function of time revealing different stages, in quantitative agreement with theory.

PACS numbers: 45.70.-n,45.70.Qj,47.20.-k

I. INTRODUCTION

The question whether or not the weight of a running hourglass as shown by a scale differs from the weight of the hourglass at rest is of great pedagogical value since experience shows that this question leads to controversial and instructive discussions. In our opinion, it teaches that a systematic analysis of a physical situation is superior to a phenomenological analysis, in a certain sense.

Phenomenologically, when the sand starts pouring, part of it is freely falling, thus, not supported by the balance leading to a reduced weight shown by the scale. When the grains arrive at the bottom, they come to rest in the lower chamber by transferring momentum and consequently force to the balance. A simple calculation shows that both forces sum up to zero, thus, it may be argued that except for short intervals of time in the very beginning and the very end of the flow, the scale shows the same weight as if the sand were at rest. It has been shown that this argument is wrong (or insufficient), nevertheless, it is taught till today in highschools and universities. Interestingly, this solution can be found in well recognised textbooks and journals, e.g. [1, 2] to mention just two out of many. It made it even to the National Physics Olympiad of Singapore [3].

A related problem is the change of weight of an Atwood machine when it is brought to motion. This classical experiment by Poggendorff [4] (repeated many times in the literature, e.g. [5, 6]) can be explained easily by evaluating the acceleration of the center of mass. Thus, the idea which leads us immediately to the correct solution is simple enough: Look to the acceleration of the center of mass of the hourglass! This more systematic approach reveals that the solution sketched above fails at least for the following arguments:

a) The material in the upper container and in the free falling jet is not at rest, but sand of time-dependent mass moves with a certain velocity determined by the outflow rate and the geometry of the container. Thus, in the course of time, moving material (in the upper container) comes to rest at a different location (in the lower container) which implies an acceleration.

b) At a given time t, during the small interval of time dt, sand moves effectively from a certain height h_u to h_l (see Fig. 1) where $h_u - h_l$ is a decreasing function of time. This corresponds to an acceleration whose time dependence is determined by the geometrical shape of the hourglass.

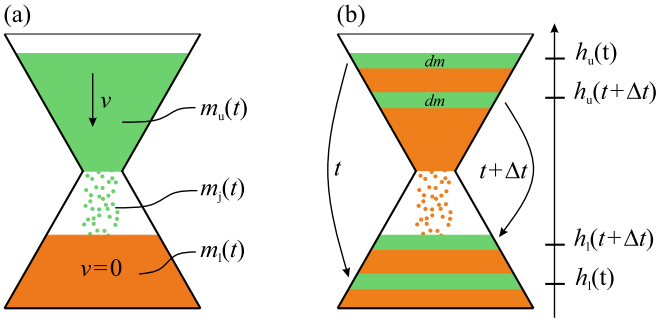

FIG. 1: (a) In an hourglass, the mass of moving material in the upper container and in the jet (green) changes over the course of time. This material comes to rest in the lower container, exerting a force during deceleration. (b) In the regime of steady flow, during time dt effectively the mass dm is transferred from $h_u(t)$ to $h_l(t)$, where $\Delta h \equiv h_u - h_l$ is a function of time and depends on the geometry of the hourglass. This implies accelerated motion of mass and, thus, a time dependent force.

From the analysis of the motion of the center of mass [7–10] follows that the weight of the hourglass is a function of time which depends on the specific details such as geometric shape of the hourglass, outflow rate, angle of repose and others. In the literature, the effect was described as tiny which can be even overcompensated by the change of gravity when turning the hourglass, thus, changing the distance of the center of mass of the sand from the center of Earth [8] which is in the order of some μg and cannot be measured with usual physics lab equipment. Even for a very large device of height 120 cm emptying in 10 s, a maximal change in weight of only 49 mg

was measured [7], but the time dependence of this effect could not be determined. Using a multiple-orifice setup [10] where the upper cylindrical container was separated from the lower cylindrical container by a sieve, a quantitative measurement was presented. For the given geometry, however, a constant increase of the weight is expected from theory whereas the measurement shows a clear trend which may be understood either from the large uncertainty (error bars) of the measurement or from the non-stationary flow rate. Indeed, unlike fluids granular matter shows flows at a rate independent of the filling height. However, whether this result shown for a single orifice using different approaches [11–13] holds true also for a flow through a sieve remains unclear. But even for the simplified experiment [10] not the full time dependence of the change of weight could be measured due to perturbations of the opening mechanism.

Here we present experimental results for the change of the weight of a hourglass as a function of time. We observe different stages of behavior which can be understood by comparison with high speed video recording and which are in *quantitative* agreement with theory based on the accelerated motion of the center of mass.

In Sections II and III we will present the experimental results and the corresponding theory, respectively. Section IV discusses the stages of the flow apparent in the time dependence of the change of mass of the hourglass. Unlike earlier references, we will show that even with simple equipment we can obtain the weight of the hourglass as a function of time and explain this function theoretically.

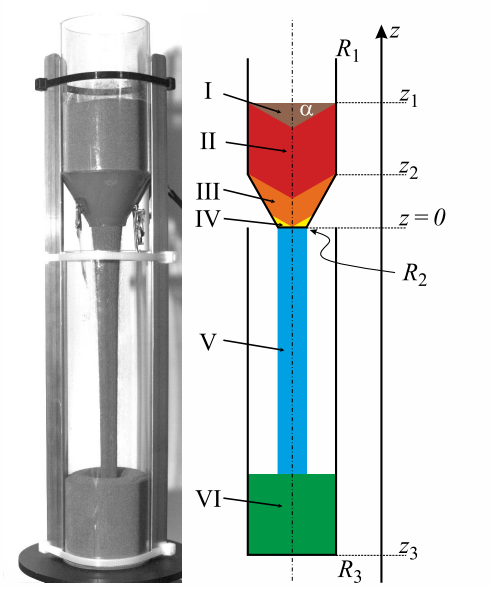

FIG. 2: Experimental setup (left). The sketch (right) introduces the geometric parameters and defines the sub-volumina I – VI where α is the angle of repose. The sketch shows a cut through the symmetry axis.

II. EXPERIMENT

The experiment is shown in Fig. 2. The upper container consists of a cylinder and a cone characterized by $R_1 = 2.75\,\mathrm{cm}$, $R_2 = 1.0\,\mathrm{cm}$, and $Z_2 = 3.5\,\mathrm{cm}$, initially filled up to $Z_1 = 8.2\,\mathrm{cm}$ with $M = 800\,\mathrm{g}$ bronze powder of density $\rho = 5,230\,\mathrm{kg/m^3}$, grain size of approximately $150\,\mu\mathrm{m}$ and angle of repose of $\alpha = 28.3\,^\circ$. This filling material was chosen for its high density and in order to avoid electrical charging of the material leading to a homogeneous flow. The lower compartment consists of a cylinder characterized by $R_3 = 2.75\,\mathrm{cm}$ and $Z_3 = -21.5\,\mathrm{cm}$. Both upper and lower compartments are manufactured from polycarbonate material. Unlike common hourglasses, we did not seal the upper and lower vessel in order to avoid a difference of air pressure in the upper and lower compartments: In closed, non-evacuated hourglasses the flow of sand through the orifice carries a small amount of air with it leading to increased pressure of air in the lower chamber [14]. It was shown that the counter-flowing air leads to unsteady flow termed "ticking of hourglasses" which was extensively studied in the literature [15–19]. The open construction of our experiment avoids pressure differences by flowing air and, thus, provides a steady flow of sand at rate $F = 720\,\mathrm{g/s}$.

The hourglass was placed on a balance using a load cell with 2 kg capacity (LCB70, ME-Meßsysteme). The electrical signal from the strain gauge of the load cell was amplified and digitized using an ADS1281 analog-to-digital converter. The weight of the hourglass was sampled at rate $250\,\mathrm{s^{-1}}$.

Initially, the orifice of the upper container was closed by a lid held by an electromagnet. At time $t = 0$ the orifice was opened and the pouring sand led to an accelerated motion of the center of mass and, thus, to a chance of the weight measured by the balance. Fig. 3 shows the weight of the hourglass during the run where the mass of the apparatus was subtracted. A running average over 6 samples was applied to suppress high frequency oscillations inevitably appearing due to the finite stiffness of the load cell.

A movie of the measurement is provided as supplementary material [20]. The details of the experimental result will be discussed below. In the following section we compute the weight of the hourglass theoretically with some model assumptions. Comparing experiment and theory in Sec. IV we will obtain quantitative agreement.

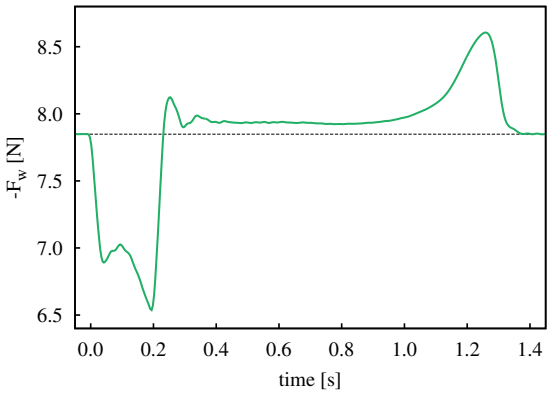

FIG. 3: Weight of the granulate inside the hourglass as a function of time (the weight of the apparatus subtracted). At time $t = 0$ the orifice opens. We observe a characteristic evolution which can be understood in detail from the theory presented in Sec. III.

III. MODEL

A. Geometry

The geometry of our model hourglass is sketched in Fig. 2. As for a typical hourglass, the upper container consists of a cone and a cylinder. The lower container is symmetrical, however, we assume that the total volume of the sand only fills the cylindrical portion of the container, such that we do not need to describe the lower cone in our calculation.

For the computation of the vertical position of the center of mass (COM), $Z(t)$, we subdivide the volume into sub-volumina I − VI of time-dependent mass and center of mass, $m_i(t)$ and $Z_i(t)$, $(i = \mathrm{I}, \ldots, \mathrm{VI})$, respectively, with

$$Z(t) = \frac{\sum_{i=\mathrm{I}}^{\mathrm{VI}} Z_i(t) m_i(t)}{\sum_{i=\mathrm{I}}^{\mathrm{VI}} m_i(t)} = \frac{1}{M} \sum_{i=\mathrm{I}}^{\mathrm{VI}} Z_i(t) m_i(t)\,, \qquad (1)$$

with M being the total mass of the sand. Knowing $Z(t)$ as an analytic function, we can compute the time dependent force acting on the balance,

$$F_w = M \left(g + \frac{\mathrm{d}^2 Z(t)}{\mathrm{d}t^2} \right) . \qquad (2)$$

The masses and centers of mass of the sub-volumina are functions of time of the form

$$m_i(t) = \begin{cases} m_i^0 = \text{const.} & \text{for } \; t \le t_i^0 \\ m_i'(t) & \text{for } \; t_i^0 \le t \le t_i^{\mathrm{e}} \\ m_i^{\mathrm{e}} = \text{const.} & \text{for } \; t \ge t_i^{\mathrm{e}} \end{cases} \quad i = \mathrm{I} \ldots \mathrm{VI} \qquad (3)$$

$$Z_i(t) = \begin{cases} Z_i^0 = \text{const.} & \text{for } \; t \le t_i^0 \\ Z_i'(t) & \text{for } \; t_i^0 \le t \le t_i^{\mathrm{e}} \\ Z_i^{\mathrm{e}} = \text{const.} & \text{for } \; t \ge t_i^{\mathrm{e}} \end{cases} \quad i = \mathrm{I} \ldots \mathrm{VI}\,. \qquad (4)$$

For the initial conditions we assume that the upper container is filled up to the hight z_1 and the upper surface of the granular material is flat. At time $t = 0$ the material starts flowing through the orifice at rate F. In contrast to a fluid, the pressure at the orifice and, thus, the flow rate F are independent of the filling hight [21–31], known as Janssen's law [32] and Beverloo's law [11], respectively. From a dimension analysis [33, 34] follows the functional form of the flow rate,

$$F = \frac{dm}{dt} = C_F \sqrt{g} \rho A^{5/4}\,, \qquad (5)$$

with the dimensionless constant C_F, where g and ρ are gravity and material density and A is the cross section of the orifice. In this paper, we assume that the flow F is independent of time as long as sand flows. This is a good approximation except, perhaps, for the very first instant where the acceleration of the granulate is limited by inertia of the sand and the very last moment when the filling height of the upper container is in the order of the diameter of the orifice. For the quantitative comparison in Sec. IV we measured the value of F under this assumption.

In the following Sections, III B-III F, we compute m_i and Z_i and the corresponding times t_i^0 and t_i^{e} for all sub-volumina and subsequently in Sec. IV the function $Z(t)$ and the corresponding weight of the hourglass.

For the calculation, we will introduce the time dependent filling level, $z(t)$, defined as the highest vertical position occupied by sand, and some temporary variables, indicated by an asterisk, e.g., x^*. Such variables are only relevant in the context of the present section.

For the quantitative plots we assume the parameters $g = -9.81\,\mathrm{m/s^2}$, $\rho = 5,230\,\mathrm{kg/m^3}$, $R_1 = 2.75\,\mathrm{cm}$, $R_2 = 1.0\,\mathrm{cm}$, $z_1 = 8.2\,\mathrm{cm}$, $z_2 = 3.5\,\mathrm{cm}$, $\alpha = 28.3°$, and $F = 0.69\,\mathrm{kg/s}$, in agreement with the experiment, Sec. II.

B. Sub-Volume I (brown)

At initial time, $t = 0$, volume I (brown in Fig. 2) has the shape of a cone. Obviously,

$$m_{\mathrm{I}}^0 = \frac{\rho\pi}{3} R_1^3 \tan\alpha\,; \quad t_{\mathrm{I}}^0 = 0\,; \quad t_{\mathrm{I}}^{\mathrm{e}} = \frac{m_{\mathrm{I}}^0}{F}\,,$$
$$m_{\mathrm{I}}^{\mathrm{e}} = 0\,; \quad m_{\mathrm{I}}'(t) = m_{\mathrm{I}}^0 - Ft\,; \quad Z_{\mathrm{I}}^0 = z_1 - \frac{1}{4} R_1 \tan\alpha \qquad (6)$$

There are two possible scenarios for the emptying of volume I: In case (a), see Fig. 4a, a crater of constant slope α is forming in the middle of the volume. The crater grows until its radius approaches R_1 at $t = t_{\mathrm{I}}^{\mathrm{e}}$. In case

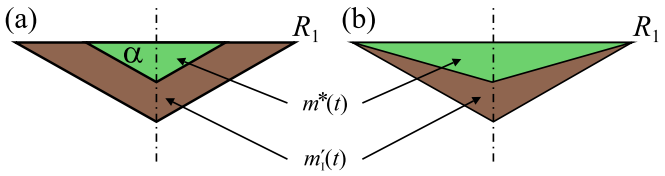

FIG. 4: Scenarios (a) and (b) for the outflow of volume I.

(b), see Fig. 4b, a crater of radius R_1 and increasing depth forms. At $t = t_{\rm I}^{\rm e}$, its slope approaches the angle of repose, α. For both cases, we describe the brown-shaded body in Fig. 4 as superposition of the initial cone whose mass and center of mass given by Eq. (6) and the green cone of (negative) mass $m^*(t) = -Ft$ and COM

$$Z^*(t) = \begin{cases} z_1 - \frac{1}{4}\left(\frac{3F\tan^2\alpha}{\rho\pi}\right)^{1/3} t^{1/3} & \text{case (a)} \\ z_1 - \frac{3}{4}\frac{F}{\rho\pi R_1^2} t & \text{case (b)}\,. \end{cases} \tag{7}$$

The COM of volume I for $t_{\rm I}^0 \le t \le t_{\rm I}^{\rm e}$ is then

$$Z_{\rm I}'(t) = \frac{1}{m_{\rm I}'(t)}\left[Z_{\rm I}^0 m_{\rm I}^0 + Z^*(t)m^*(t)\right]\,. \tag{8}$$

Figure 5 shows $Z_{\rm I}$ for both cases. It may surprise that

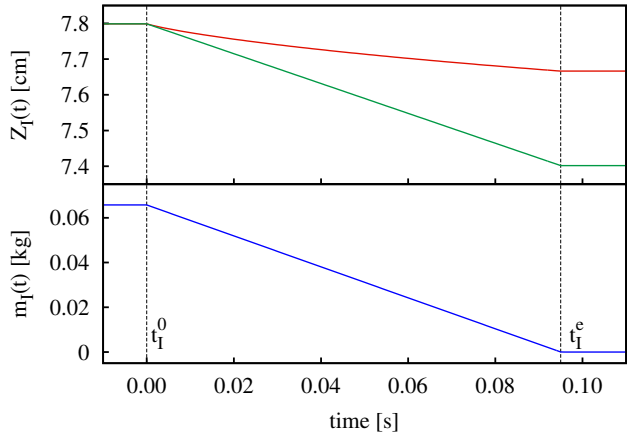

FIG. 5: COM for scenarios (a) and (b) (top) and Mass (bottom) of volume I as functions of time.

the limits $t \to t_{\rm I}^{\rm e}$ are different for both cases. When we express for case (a) $Z_{\rm I}'(t)$ as a function of the instantaneous radius, r^*, of the smaller cone we obtain

$$Z_{\rm I}^{\rm e} = \lim_{r^*\to R_1} z_1 - \frac{\tan\alpha}{4}\frac{R_1^4 - (r^*)^4}{R_1^3 - (r^*)^3} = z_1 - \frac{R_1\tan\alpha}{3} \tag{9}$$

For case (b) we express $Z_{\rm I}(t)$ in terms of the position z of the tip of the smaller cone. Here we obtain

$$\begin{aligned} Z_{\rm I}^{\rm e} &= \lim_{z\to z_1 - R_1\tan\alpha} z_1 - \frac{1}{4}\left(z_1 - R_1\tan\alpha - z\right) \\ &= z_1 - \frac{R_1\tan\alpha}{2}\,, \end{aligned} \tag{10}$$

see Fig. 5. The different limits are an interesting mathematical peculiarity which has its origin ultimately in the continuum description of granular matter which is problematic in the limit of mass approaching zero. For our calculation, it is, however, unproblematic since in the same limit mass vanishes, $m_{\rm I}(t) \to 0$ for $t \to t_{\rm I}^{\rm e}$, therefore, the product, $m_{\rm I}(t)Z_{\rm I}(t)$, does not contribute to Eq. (1) for $t \ge t_{\rm I}^{\rm e}$.

C. Sub-Volume II (red)

Initially, volume II, see Fig. 2, consists of a cylinder of height $z_1 - z_2$ and radius R_1, closed at the top by a cone of negative mass and an identical cone but of positive mass at the floor. Thus,

$$\begin{aligned} &m_{\rm II}^0 = \pi R_1^2(z_1 - z_2)\,; \quad t_{\rm II}^0 = t_{\rm I}^{\rm e}\,; \quad t_{\rm II}^{\rm e} = t_{\rm II}^0 + \frac{m_{\rm II}^0}{F} \\ &m_{\rm II}'(t) = M_{\rm II}^0 - \left(t - t_{\rm II}^0\right)F\,; \quad m_{\rm II}^{\rm e} = 0 \end{aligned} \tag{11}$$

For $t_{\rm II}^0 \le t \le t_{\rm II}^{\rm e}$, the filling level reads

$$z(t) = z_1 - \frac{F}{\rho\pi R_1^2}\left(t - t_{\rm II}^0\right) \tag{12}$$

and we write for the COM of the cylinder

$$Z_{\rm cyl}^*(t) = \frac{z(t) + z_2}{2}\,. \tag{13}$$

For the upper and lower cones we obtain

$$\begin{aligned} m_{\rm cu}^* &= -\frac{\rho\pi}{3}R_1^3\tan\alpha\,; \quad Z_{\rm cu}^*(t) = z(t) - \frac{R_1\tan\alpha}{4} \\ m_{\rm cl}^* &= -m_{\rm cu}^*\,; \quad Z_{\rm cl}^*(t) = z_2 - \frac{R_1\tan\alpha}{4}\,. \end{aligned} \tag{14}$$

Consequently,

$$\begin{aligned} Z_{\rm II}' &= \frac{1}{m_{\rm II}'}\left[m_{\rm II}' Z_{\rm cyl}^* + m_{\rm cu}^* Z_{\rm cu}^* + m_{\rm cl}^* Z_{\rm cl}^*\right] \\ &= \frac{z(t) + z_2}{2} - \frac{R_1\tan\alpha}{3} \end{aligned} \tag{15}$$

and in particular

$$Z_{\rm II}^0 = \frac{z_1 + z_2}{2} - \frac{R_1\tan\alpha}{3}\,; \quad Z_{\rm II}^{\rm e} = z_2 - \frac{R_1\tan\alpha}{3}\,. \tag{16}$$

Figure 6 shows the functions $Z_{\rm II}(t)$ and $m_{\rm II}(t)$.

D. Sub-Volume III (orange)

Volume III is given by the orange region in Fig. 2 and the magnification in Fig. 7 where the nomenclature used in this section is introduced. We define the conical segments $S_1, \ldots, S_4$ of negative an positive masses whose superposition equals volume III. Note that only S_3 and S_4 depend on time.

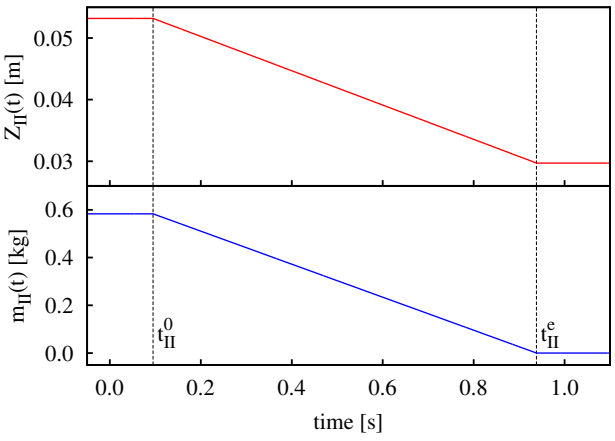

FIG. 6: COM (top) and Mass (bottom) of volume II as functions of time.

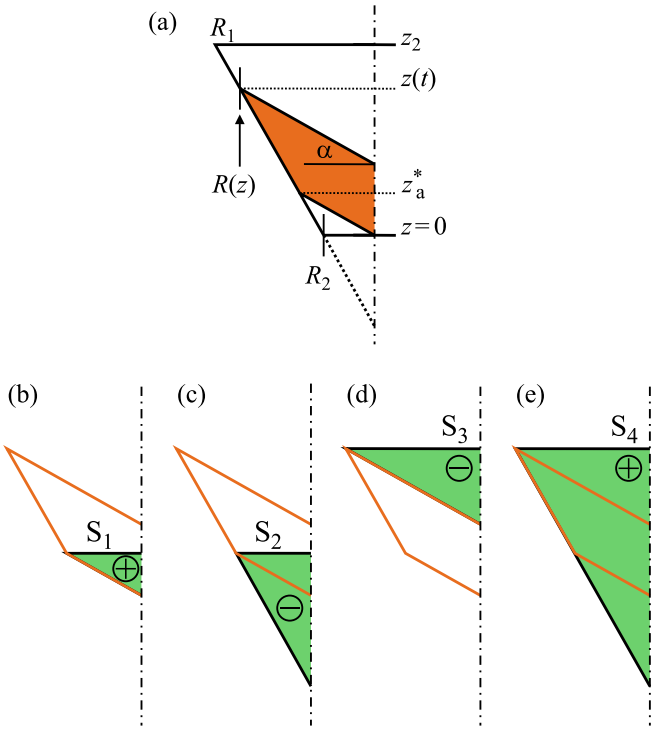

FIG. 7: (a) Sketch of the sub-volume III (orange) to introduce the nomenclature. (b-e) Segments of volumes of positive ⊕ and negative ⊖ masses used in the calculation. Their superposition results in volume III.

1. *Segment S_1*

Sub-volume S_1 (see Fig. 7) is a time-independent cone of positive mass of height and radius

$$z_a^* = \frac{R_2}{T}\,; \qquad R(z_a^*) = \frac{z_a^*}{\tan\alpha}\,, \tag{17}$$

respectively, where we define for later reference

$$T \equiv \frac{1}{\tan\alpha} - \frac{R_1 - R_2}{z_2}\,. \tag{18}$$

Consequently

$$m_1^* = \frac{\rho\pi}{3\tan^2\alpha}\left(\frac{R_2}{T}\right)^3\,; \qquad Z_1^* = \frac{3}{4}\frac{R_2}{T}\,. \tag{19}$$

2. *Segment S_2*

Segment S_2 is a time-independent cone of negative mass with the same radius as S_1 and height $z_a^* + z_2R_2/(R1-R2)$, thus, with Eq. (17)

$$\begin{aligned} m_2^* &= -\frac{\rho\pi}{3\tan^2\alpha}\left(\frac{R_2}{T} + \frac{z_2R_2}{R1-R2}\right)^3 \\ Z_2^* &= \frac{R_2}{T} - \frac{1}{4}\left(\frac{R_2}{T} + \frac{z_2R_2}{R1-R2}\right)\,. \end{aligned} \tag{20}$$

3. *Segment S_3*

Segment S_3 of negative mass is a cone with radius $R(z)$ and height $R(z)\tan\alpha$, therefore, for $t^0_{\rm III} = t^{\rm e}_{\rm II} \le t \le t^{\rm e}_{\rm III}$:

$$\begin{aligned} m_3^*(z) &= -\frac{\pi\rho}{3}\left[R_2 + \frac{R1-R2}{z_2}z(t)\right]^3\tan\alpha \\ Z_3^*(z) &= z(t) - \frac{\tan\alpha}{4}\left[R_2 + \frac{R1-R2}{z_2}z(t)\right]\,. \end{aligned} \tag{21}$$

The filling height $z(t)$ and $t^{\rm e}_{\rm III}$ are computed later from the total mass of sub-volume III. For $t \to t^0_{\rm III}$ when $z \to z_2$, we obtain

$$m_3^*(z_2) = -\frac{\pi\rho}{3}R_1^3\tan\alpha\,; \quad Z_3^*(z_2) = z_2 - \frac{1}{4}\tan\alpha R_1\,. \tag{22}$$

4. *Segment S_4*

Segment S_4 is a cone of mass and COM given by

$$\begin{aligned} m_4^*(z) &= \frac{\pi\rho}{3}\left[R_2 + \frac{R_1-R_2}{z_2}z(t)\right]^2\left[z(t) + \frac{z_2R_2}{R_1-R_2}\right] \\ Z_4^*(z) &= \frac{3}{4}z(t) - \frac{1}{4}\frac{z_2R_2}{R_1-R_2} \end{aligned} \tag{23}$$

The first bracket in Eq. (23) specifies the radius $R(z(t))$ of the cone, and the second bracket is its height. The initial mass and COM follow for $z \to z_2$,

$$\begin{aligned} m_4^*(z_2) &= \frac{\pi\rho}{3}R_1^2z_2\left[1 + \frac{R_2}{R_1-R_2}\right] \\ Z_4^*(z_2) &= \frac{z_2}{4}\left[3 - \frac{R_2}{R_1-R_2}\right] \end{aligned} \tag{24}$$

5. Mass and COM of Sub-Volume III

Using the results of the previous sections, we compute mass and COM of volume III by superposition of the segments $S_1, \ldots, S_4$. From the initial mass in segment III

$$m^0_{\rm III} = m^*_1 + m^*_2 + m^*_3(z_2) + m^*_4(z_2) = F\,\left(t^{\rm e}_{\rm III} - t^0_{\rm III}\right)\,, \tag{25}$$

and because obviously $m^{\rm e}_{\rm III} = 0$, we obtain the time $t^{\rm e}_{\rm III}$. The total mass as a function of time then follows from

$$m_{\rm III}(t) = m^0_{\rm III} - F\,\left(t - t^0_{\rm III}\right) \tag{26}$$

For the computation of the COM via the COM's of the segments,

$$Z'_{\rm III}(t) = \frac{1}{m'_{\rm III}(t)}\,(Z^*_1 m^*_1 + Z^*_2 m^*_2 + Z^*_3(z) m^*_3(z) + Z^*_4(z) m^*_4(z)) \tag{27}$$

we need the filling height, $z(t)$, since m^*_3, m^*_4, Z^*_3, and Z^*_4 depend on time through $z(t)$. The filling height can be found from

$$m_{\rm III}(t) = m^*_1 + m^*_2 + m^*_3(z(t)) + m^*_4(z(t))\,, \tag{28}$$

with the segment masses given by Eqs. (19, 20, 21, 23) and the time dependent mass given by Eq. (26). The lhs is a polynomial of third order of the filling height. By solving the third order equation, we obtain $z(t)$ and subsequently $Z'_{\rm III}$ as an explicit function of time via Eq. (27). Figure 6 shows the resulting functions $Z_{\rm III}(t)$ and $m_{\rm III}(t)$.

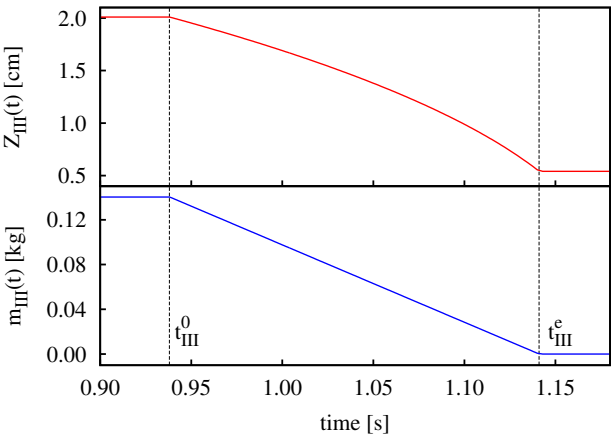

FIG. 8: COM and Mass of volume III as functions of time.

E. Sub-Volume IV (yellow)

1. Time independent flow rate

Sub-volume IV is a tiny annulus below volume III which is hardly visible in Fig: 2. The magnification, Fig. 9 defines the variable z^*_a which is the same as in Sec. III D. One can argue whether it is necessary to compute the contribution of this sub-volume since its mass is small and the computation requires some effort. We believe it is necessary for the sake of consistency. Recall that we need the second derivative of the COM to obtain the weight of the hourglass, see Eq. (2), thus, even small discontinuities may lead to large errors. For $t \ll t^0_{\rm IV}$ the area at $z = 0$ is covered with sand such that Beverloo's law, Eq. (5), ist a good approximation. For $t \approx t^0_{\rm IV}$ it is certainly not justified to assume constant flux, F, however in absence of solutions in the literature for this situation, we assume also here constant flux F. Moreover, sub-volume IV is certainly tiny as compared to all other sub-volumes such that the details of the flow regarding this volume are of minor importance for the total weight of the hourglass, provided large jumps in the second derivative are avoided, see above.

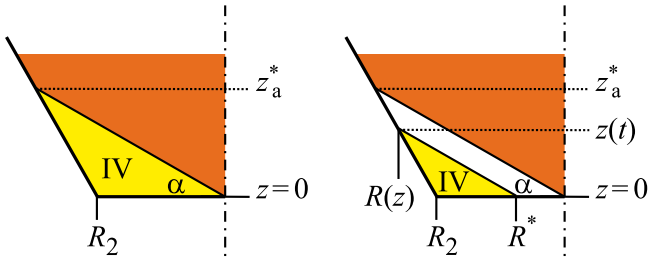

FIG. 9: Sketch of sub-volume IV (yellow). Part of sub-volume III is shown in yellow.

2. Mass of sub-volume IV

Sub-volume IV is a frustum (height $z(t)$, radii $R(z)$ and R_2) of positive mass and frustum (height $z(t)$, radii $R(z)$ and R^*) of negative mass, see Fig. 9. Its mass ist, therefore,

$$\frac{m'_{\rm IV}(t)}{\rho\pi} = \frac{z}{3}\left[R^2(z) + R(z)R_2 + R_2^2\right] - \frac{z}{3}\left[R^2(z) + R(z)R^* + (R^*)^2\right] \tag{29}$$

with

$$R(z) = R_2 + z(R1 - R2)/z_2\,, \quad R^* = R_2 - zT\,, \tag{30}$$

with T defined in Eq. (18). Then

$$\frac{m_{\mathrm{IV}}(t)}{\rho\pi} = TR_2z^2 + \frac{1}{3}T\left(\frac{R_1-R_2}{z_2} - T\right)z^3\,. \qquad (31)$$

At time $t^0_{\mathrm{IV}} = t^{\mathrm{e}}_{\mathrm{III}}$ we have $z = z^*_a$ and Eq. (31) simplifies to

$$m^0_{\mathrm{IV}} = \rho\pi R_2^3\left(\frac{1}{T} - \frac{1}{3\tan\alpha T^2}\right)\,. \qquad (32)$$

We obtain the mass of sub-volume IV:

$$m'_{\mathrm{IV}}(t) = m^0_{\mathrm{IV}} - F\left(t - t^0_{\mathrm{IV}}\right)\,; \quad t^{\mathrm{e}}_{\mathrm{IV}} = t^0_{\mathrm{IV}} + \frac{m^0_{\mathrm{IV}}}{F} \qquad (33)$$

and $m^{\mathrm{e}}_{\mathrm{IV}} = 0$.

3. *COM of sub-volume IV*

For the computation of the COM we need the filling height $z(t)$ in explicite terms which can be obtained by solving a third-order equation obtained from equating $m'_{\mathrm{IV}}(t)$ in Eqs. (31) and (33).

With $z(t)$, the COM of sub-volume IV (frustum) is given by

$$Z'_{\mathrm{IV}}(t) = \frac{z(t)}{4}\frac{R^2(z) + 2R(z)R_2 + 3R_2^2}{R^2(z) + R(z)R_2 + R_2^2} \qquad (34)$$

and $Z^{\mathrm{e}}_{\mathrm{IV}} = \lim_{z\to 0} Z'_{\mathrm{IV}} = 0$. Figure 10 shows the functions $Z_{\mathrm{IV}}(t)$ and $m_{\mathrm{IV}}(t)$.

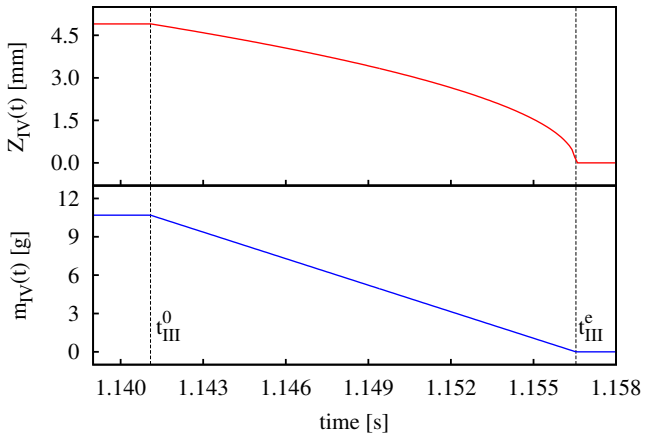

FIG. 10: COM and mass of volume IV as functions of time.

F. Sub-volumes V and VI (blue and green)

The calculations for subvolumes V and VI (jet and lower container) are closely related, therefore, we present them together in this section. Sub-volume V is the falling jet bound by the orifice at $z = 0$ and the filling level $z_l(t)$ of the lower container. Sub-volume VI consists of the sand resting in the lower container which is a cylinder of radius R_3 with the lower bottom at z_3, see Fig. 2. Based on the experimental observation [20] we assume that the upper surface of the sand is flat owed to the large flow rate in our experiment. The same calculation can be performed for a certain angle of repose. The close relation of the sub-volumes originate from the fact that their common boundary changes with time. Indeed, the surface at vertical position $z_l(t)$ moves upwards in time, therefore, despite constant flow rate, F, the rate of sand settling at the floor is different from F.

1. *Density, mass and COM of the jet in general*

Particles enter volume V at a certain initial velocity, v^*, which follows from continuity between volumes IV and V. Since the jet is not confined by lateral walls, here we cannot rely on Beverloo's law [11] but assume that the flow is proportional to its cross-section, thus

$$v^* = -\frac{F}{\rho\pi R_2^2}\,. \qquad (35)$$

At time $t = 0 = t^0_{\mathrm{V}}$ the lid opens and the grains start falling at velocity v^*. Using

$$F = \frac{dm}{dt} = \frac{dm}{dz}\frac{dz}{dt} = \frac{dm}{dz}v(z) \qquad (36)$$

we compute the density of the jet $\mathrm{d}m/\mathrm{d}z$. The velocity of the grains at vertical position z is

$$v(z) = -\sqrt{(v^*)^2 + 2gz}\,, \qquad (37)$$

thus,

$$\frac{dm}{dz} = -\frac{F}{\sqrt{(v^*)^2 + 2gz}}\,, \qquad 0 \geq z \geq z_l \qquad (38)$$

with the filling height, $z_l(t)$, given below.

With the yet unspecified upper and lower boundaries of the jet, z_L and z_U, respectively, we obtain general equations for the mass of the jet,

$$\begin{aligned} m_{\mathrm{jet}}\left(z_{\mathrm{L}}, z_{\mathrm{U}}\right) &= \int_{z_{\mathrm{L}}}^{z_{\mathrm{U}}}\frac{\mathrm{d}m}{\mathrm{d}z}\mathrm{d}z \\ &= \frac{F}{g}\left[\sqrt{(v^*)^2 + 2gz_{\mathrm{U}}} - \sqrt{(v^*)^2 + 2gz_{\mathrm{L}}}\right] \end{aligned} \qquad (39)$$

and the COM:

$$Z_{\rm jet}\left(z_{\rm L},z_{\rm U}\right)=\frac{1}{m_{\rm jet}\left(z_{\rm L},z_{\rm U}\right)}\int_{z_{\rm L}}^{z_{\rm U}}z\frac{dm}{dz}dz$$
$$=-\frac{F}{3g^2\,m_{\rm jet}\left(z_{\rm L},z_{\rm U}\right)}\left[\left(z_{\rm L}g-\left(v^*\right)^2\right)\sqrt{\left(v^*\right)^2+2z_{\rm L}g}\right.$$
$$\left.-\left(z_{\rm U}g-\left(v^*\right)^2\right)\sqrt{\left(v^*\right)^2+2z_{\rm U}g}\right] \quad (40)$$

2. *Vertical Position of the Interface Between Volumes V and VI, $z_l(t)$*

Sub-volume VI becomes active when the first grain arrives at the floor at position z_3 at time

$$t^0_{\rm VI}=\frac{1}{g}\left(\sqrt{\left(v^*\right)^2+2gz_3}-v^*\right)\,. \quad (41)$$

For $0=t^0_{\rm V}\le t\le t^{\rm e}_{\rm IV}$, the mass flown through the orifice until a certain time is either located in the jet or as a sediment in the lower container:

$$F\,t=\pi R_3^2 z_l+m_{\rm jet}\left(z_l,0\right)\,. \quad (42)$$

With Eq. (39) for $m_{\rm jet}$ we obtain a quadratic equation for $z_l(t)$.

3. *Mass and COM of Sub-Volume V (jet)*

Using the general results from Secs. III F 1 and III F 2 we can compute the evolution of mass and center of mass position of volume V. The scenario is the following: at time $t=0$, the lid opens and the jet gains mass rapidly. The first grain hits the floor at z_3 short time after. From this moment on, the mass of the jet decreases slowly since the lower filling level, z_l, increases. When the last grain enters the jet at the orifice, the mass of the jet decreases rapidly and vanishes when the last grain arrived at the floor. In quantitative terms:

- **time** $0=t^0_{\rm V}\le t\le t^0_{\rm VI}$

$$\begin{aligned}m'_{\rm V}(t)&=m_{\rm jet}\left(-\tfrac{g}{2}t^2+v^*t\,,\,0\right)\\ Z'_{\rm V}(t)&=Z_{\rm jet}\left(-\tfrac{g}{2}t^2+v^*t\,,\,0\right)\end{aligned} \quad (43)$$

- **time** $t^0_{\rm VI}\le t\le t^{\rm e}_{\rm IV}$

$$\begin{aligned}m'_{\rm V}(t)&=m_{\rm jet}\left(z_l\,,\,0\right)\\ Z'_{\rm V}(t)&=Z_{\rm jet}\left(z_l\,,\,0\right)\end{aligned} \quad (44)$$

with $z_l(t)$ given by the solution of Eq. (42).

- **time** $t^{\rm e}_{\rm IV}\le t\le t^{\rm e}_{\rm V}$
At time $t^{\rm e}_{\rm V}$ the last grain comes to rest at vertical position $z^{\rm e}_l\equiv z_l\left(t^{\rm e}_{\rm V}\right)$. The terminal filling height, $z^{\rm e}_l$ is obtained from equating the initial mass of sand in the upper part of the hourglass with the final state, where the sand is contained in the lower part,

$$m^0_{\rm I}+m^0_{\rm II}+m^0_{\rm III}=m^{\rm e}_{\rm V} \quad (45)$$

yielding

$$z^{\rm e}_l=z_3+\frac{R_1^2}{R_3^2}\left(z_1-z_2\right)+\frac{z_2}{3}\frac{R_1^2+R_1R_2+R_2^2}{R_3^2} \quad (46)$$

and the corresponding time

$$t^{\rm e}_{\rm V}=t^{\rm e}_{\rm VI}=t^{\rm e}_{\rm IV}+\frac{1}{g}\left(\sqrt{\left(v^*\right)^2+2g\,z^{\rm e}_l}-v^*\right) \quad (47)$$

with v^* given by Eq. (35).

For completeness, we add the initial and final values: $m^0_{\rm V}=m^{\rm e}_{\rm V}=0$; the COM's $Z^0_{\rm V}$ and $Z^{\rm e}_{\rm V}$ are both undefined but finite, that is, they do not contribute to the total COM of the system. Figure 11 shows the functions $Z_{\rm V}(t)$ and $m_{\rm V}(t)$.

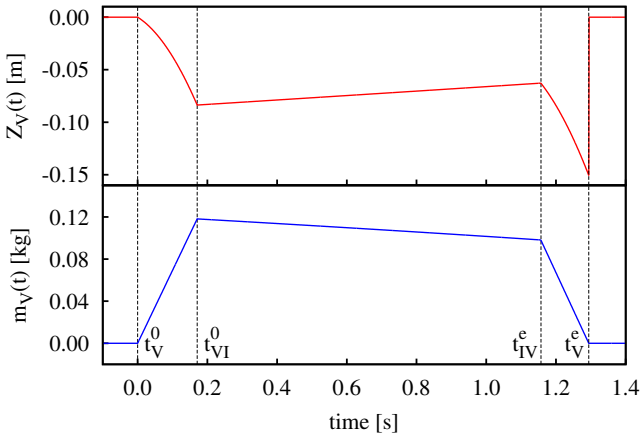

FIG. 11: COM and Mass of volume V as functions of time.

4. *Mass and COM of Sub-Volume VI (lower vessel)*

Volumes V and VI have a common interface at $z_l(t)$, therefore, $t^{\rm e}_{\rm VI}=t^{\rm e}_{\rm V}$. The mass and COM of volume VI can be directly concluded from the evolution of the lower filling height, $z_l(t)$, being the solution of Eq. (42), that is,

$$\begin{aligned}m'_{\rm VI}&=\rho\pi R_3^2\left[z_l(t)-z_3\right]\,,\\ Z'_{\rm VI}&=\tfrac{1}{2}\left[z_l(t)-z_3\right]\,.\end{aligned} \quad (48)$$

The initial and final values are

$$\begin{aligned} m^0_{\rm VI} &= 0 \\ m^{\rm e}_{\rm VI} &= m^0_{\rm I} + m^0_{\rm II} + m^0_{\rm III} \\ Z^0_{\rm VI} &\equiv \lim_{t\to+t^0_{\rm VI}} Z'_{\rm VI}(t) = z_3 \\ Z^{\rm e}_{\rm VI} &= \tfrac{1}{2}\,(z^{\rm e}_l - z_3)\ . \end{aligned} \tag{49}$$

Figure 12 shows the functions $Z_{\rm VI}(t)$ and $m_{\rm VI}(t)$.

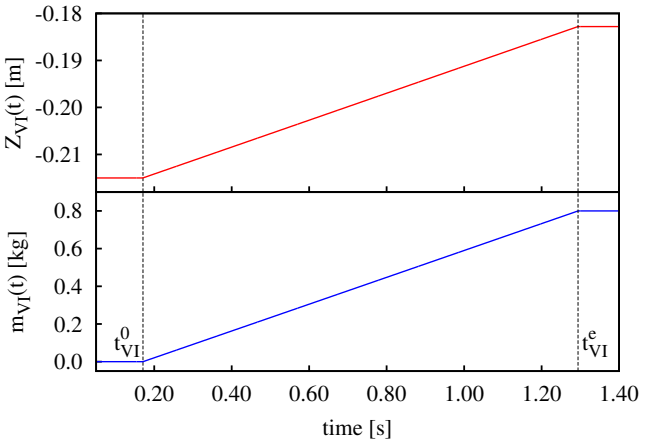

FIG. 12: COM and Mass of volume VI as functions of time.

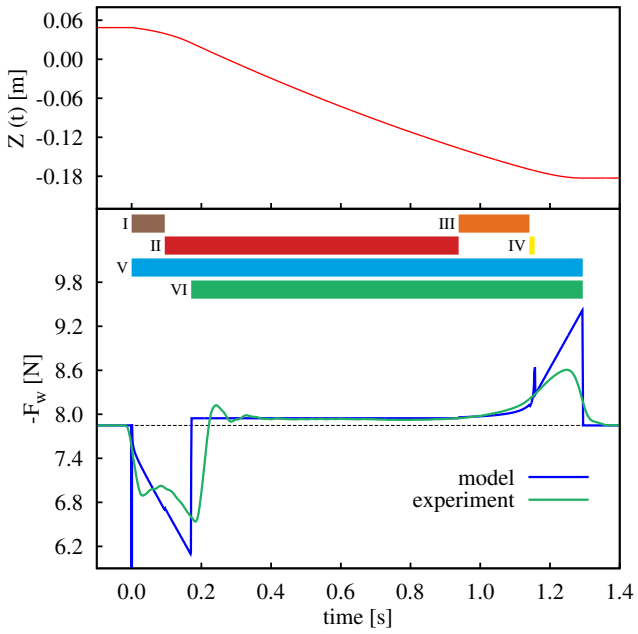

FIG. 13: Center of mass of the sand flowing in the hourglass as a function of time and weight of the hourglass derived from it due to Eq. (2). The dashed line shows the weight of the hourglass when the material is at rest. For comparison, the green line repeats the experimental result from Fig. 2. The horizontal bars indicate the intervals of time when the irrespective subvolumes are active, $(t^0_i, t^{\rm e}_i)$ with $i = \{\,{\rm I}, \ldots\, {\rm VI}\}$. Their color corresponds to the color in Fig. 2.

IV. CENTER OF MASS AND WEIGHT OF THE HOURGLASS

The total center of mass, $Z(t)$, is obtained via Eq. (1), where the masses and COMs of the sub-volumes are given in the form of Eqs. (3,4) with the details for each subvolume computed in Secs. III B-III F. The solution, $Z(t)$, obtained here is rigorous, that is, entirely analytical, albeit given in piecewise form which makes mathematical operations with this function rather cumbersome. Computer algebra systems such as MAPLE can be used to conveniently compute the second derivative of this function to obtain the weight F_w of the hourglass via Eq. (2) with the total mass given by $M = m^0_{\rm I} + m^0_{\rm II} + m^0_{\rm III}$.

Figure 13 shows the final result of the analysis, that is, the center of mass, $Z(t)$, and the force resulting from its second derivative due to Eq. (2). While $Z(t)$ appears less impressive, the force shows distinct characteristics which are similar to the experimental data: In particular, we recognise three distinct stages, (a) the initial interval, $0 < t \lesssim 0.2\,$s, where the jet and the cone develop, (b) the stage of approximately constant flow, $0.2\,{\rm s} \lesssim t \lesssim 1$s, and (c) the final stage, $t \gtrsim 1$s, when the upper vessel and the jet run empty and the material comes to rest. In all three stages we find qualitative and even partially quantitative agreement between theory (blue line) and experiment (green line) without employing any adjustable parameters in the model. In particular, in stage (b) where the textbook solution discussed in the introduction fails, we find quantitative agreement of theory and experiment.

Despite the overall good agreement of theory and experiment, there are some sizeable local deviations which shall be discussed in detail: First we notice a sharp negative peak at $t = 0$ in the theoretical curve which appears less sharp in the experimental data. The reason for this peak is the assumption that at $t = 0$ the sand starts pouring instantaneously, that is, a finite mass is set into downward motion at finite velocity instantaneously which implies a δ-shaped negative acceleration. Looking to the experimental data, we notice that there is a similar behavior, however, the negative peak is of finite value and duration due to the fact that the sand is not set into motion *instantaneously* but needs a finite time to accelerate. Reducing the total amount of sand, the mass accelerated at $t = 0$ decreases and the peak gradually disappears. Figure 14 shows the experimentally measured weight in the initial interval $t < 0.22\,$s for different amounts of granular material.

At $t \approx 0.25\,$s, in Fig. 13 we observe a damped oscillation in the experimentally measured weight which

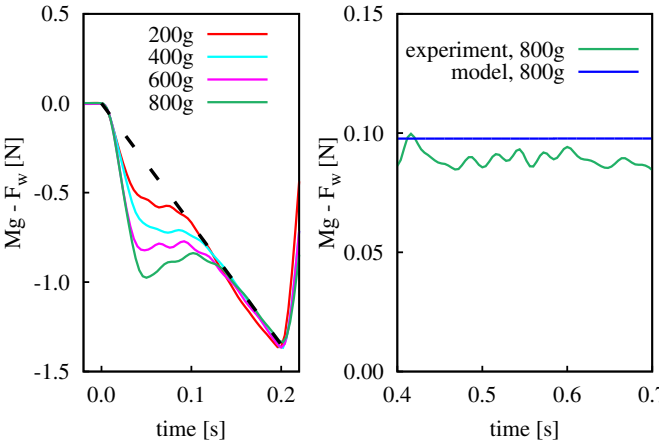

FIG. 14: Left: Experimentally measured weight in the initial interval $t < 0.22\,\mathrm{s}$ for different amounts of granular material (magnification of Fig. 13). The figure illustrates the appearance of the initial negative peak due to the acceleration of the total amount of granular material after opening the lid at $t = 0$. Right: Magnification of the plateau in Fig. 13. The deviation of the experimental and theoretical result is about 10%.

does not appear in the theoretical result. The reason for this deviation is the splash of the granular material in a short period after the instant when the jet arrives at the bottom at $t = t^0_{\mathrm{VI}}$. In the theory we assume that the material comes to rest instantaneously. The movie of the experiment [20] shows that this assumption is well justified for the entire experiment, except for a short intervall after t^0_{VI}. The small oscillations visible, e.g. in the intervall at $t = (0.05 \ldots 0.1)\,\mathrm{s}$ in Fig. 14 are due to the eigenfrequency of the balance.

A third significant deviation between experiment and theory can be seen at $t \approx t^{\mathrm{e}}_{\mathrm{VI}}$ when the experiment terminates. While theory predicts an instantaneous drop of the weight, the experiment shows a smooth decay. The reason for this deviation is the assumption of constant flow rate, F due to Beverloo's law, see discussion of Eq. (5). According to Janssen's law, the pressure and, thus, the flow rate are independent of the filling height, except when the filling height is too small and approaches the size of the orifice or even drops below it. But this is the case for $t \approx t^{\mathrm{e}}_{\mathrm{VI}}$ such that the assumption of constant flow is not justified close to the very end of the experiment. For the same reason, that is, assuming constant flow rate in the interval $(t^0_{\mathrm{IV}}, t^{\mathrm{e}}_{\mathrm{IV}})$, the small positive peak at $t = t^0_{\mathrm{IV}}$ appears, see discussion in Sec. III E 1.

V. CONCLUSION

The weight of a pouring hourglass deviates from the weight of the hourglass at rest due to the accelerated motion of the sand. While this insight is not new (but still not generally acknowledged), in several references it was claimed that the effect is tiny and hardly measurable using standard laboratory equipment. In the present paper, we perform the experiment using even sub-standard equipment and achieve quantitative agreement with theory.

While in many cases, phenomenological approaches to physics problems are successful, in the case of the weight of an hourglass it is delusive and leads to erroneous results which can be found in textbooks and lecture notes. More systematic approaches such as the one presented here, namely to consider the acceleration of the center of mass, are certainly more laborious and less elegant, however, they are certainly less prone to fail, which may be considered as the educational message of this paper.

[1] Jearl Walker. *The Flying Circus of Physics*. John Wiley & Sons, Hoboken, 1975.

[2] W. P. Reid. Weight of an hourglass. *Am. J. Phys.*, 35:351, 1967.

[3] P. P. Ong. The wavering weight of the hour-glass. *Eur. J. Phys.*, 11(3):188, 1990.

[4] J. C. Poggendorff. Ueber eine Abänderung der Fallmaschine. *Ann. Phys.*, 168(5):179–182, 1854.

[5] L. Cintra do Prado. Utilizing automatic balances for Poggendorff's experiment on the second law of motion. *Am. J. Phys.*, 38(4):541–542, 1970.

[6] R. Lopes Coelho, P. A. S. Silva, and P. de F. Borges. On the Poggendorff experiment. *Physics Education*, 50(6):667, 2015.

[7] K. Y. Shen and B. L. Scott. The hourglass problem. *Am. J. Phys.*, 53:787, 1985.

[8] I. H. Redmount and R. H. Price. The weight of time. *Phys. Teach.*, 36:432, 1998.

[9] V. Becker and T. Pöschel. Hourglass of constant weight. *Gran. Matter*, 10:231, 2008.

[10] Fokke Tuinstra and Bouke F. Tuinstra. The weight of an hourglass. *Europhysics News*, 41(3):25–28, 2010.

[11] W. A. Beverloo, H. A. Leniger, and J. van de Velde. The flow of granular solids through orifices. *Chemical Engineering Science*, 15(34):260 – 269, 1961.

[12] R. L. Brown. Minimum energy theorem for flow of dry granules through apertures. *Nature*, 191(4787):458–461, 07 1961.

[13] Metin Yersel. The flow of sand. *The Physics Teacher*, 38(5):290–291, 2000.

[14] T. Le Pennec, K. J. Måløy, A. Hansen, M. Ammi, D. Bideau, and X-L. Wu. Pressure fluctuations in ticking hour glasses. *Phys. Rev. E*, 53:2257, 1996.

[15] X. Wu, K. J. Måløy, A. Hansen, and D. Bideau. Why

hour-glasses tick. *Phys. Rev. Lett.*, 71:1363, 1993.

[16] X-l. Wu, K. J. Måløy, A. Hansen, M. Ammi, and D. Bideau. Why hour glasses tick. *Phys. Rev. Lett.*, 71:1363–1366, Aug 1993.

[17] E. Manger, T. Solberg, B.H. Hjertager, and D. Vareide. Numerical simulation of the ticking hourglass. *International Journal of Multiphase Flow*, 21(4):561 – 567, 1995.

[18] C. T. Veje and P. Dimon. Power spectra of flow in an hourglass. *Phys. Rev. E*, 56:4376, 1997.

[19] B. K. Muite, M. L. Hunt, and G. G. Joseph. The effects of a counter-current interstitial flow on a discharging hourglass. *Phys. Fluids*, 16:3415, 2004.

[20] A movie of the experiment can be found at `http://www.mss.cbi.fau.de/hg-sup/`.

[21] Huber-Burnand. Ueber das Ausfließen und den Druck des Sandes. *Ann. Phys.*, 92(6):316–328, 1829.

[22] Huber-Burnand. über den Ausfluß und den Druck des Sandes. *Z. Physik und Mathematik*, 6:95–98, 1829.

[23] Huber-Burnand. Lettre de M. Huber-Burnand à M. le professeur Prevost, sur l'écoulment et la pression du sable. *Annales de Chimie*, Junius:159–173, 1829.

[24] Huber-Burnand. über den Ausfluß und den Druk des Sandes. Schreiben des Hrn. Huber-Burnand an Hrn. Prof. Prevost. *Polytechnisches Journal*, 34:270–280, 1829.

[25] Huber-Burnand. Lettre de M. Huber-Burnand à M. le professeur Prevost, sur l'écoulment et la pression du sable. *Bibliothèque universelle des sciences, belles-lettres, et arts Genève*, 40:22–40, 1829.

[26] Huber-Burnand. Ueber den Ausfluß und den Druck des Sandes. *Kunst- und Gewerbeblatt des Polytechnischen Vereins für das Königreich Bayern*, 15:730–740, 1829.

[27] Huber-Burnand. *Repertorium der Experimentalphysik, enthaltend eine vollständige Zusammenstellung der neueren Fortschritte dieser Wissenschaft*, volume 1, supplement zu neuern Lehr- und Wörterbüchern der Physik von Gustav Theodor Fechner Ausfluß des Sandes, pages 82–84. Leopold Voß, Leipzig, 1832.

[28] T. S. Brown (Lieut. of the Corps of Engineers). Experiments on the resistance of sand to motion through tubes, with especial reference to its use in the blasting of rocks, made at Fort Adams, Newport harbour, under direction of Col. Totten. *J. Franklin Institute of the State of Pennsylvania*, 18:1–8, 1836. Uebersetzung des Briefes von Huber-Burnand.

[29] G. H. L. Hagen. über den Druck und die Bewegung des trockenen Sandes. *Bericht über die zur Bekanntmachung geeigneten Verhandlungen der Königlich Preussischen Akademie der Wissenschaften zu Berlin.*, pages 35–42, 1852.

[30] P. Forchheimer. *Über Sanddruck und Bewegungs-Erscheinungen im Inneren trockenen Sandes*. PhD thesis, Eberhard-Carls-Universität, Tübingen, 1883.

[31] B. P. Tighe and M. Sperl. Pressure and motion of dry sand: translation of Hagens paper from 1852. *Gran. Matter*, 9:141–144, 2007.

[32] H. A. Janssen. Versuche über Getreidedruck in Silozellen. *Z. Ver. Dt. Ing.*, 39:10451049, 1895.

[33] R. M. Nedderman. *Statics and Kinematics of Granular Materials*. Cambridge University Press, Cambridge, 1992.

[34] H. Fischler and R. Corati. Himmelsblau und Sanduhr: Die heuristische Kraft der Dimensionsanalyse. *Physik in der Schule*, 33:12, 1995.